Astronomy & Astrophysics manuscript no. aanda
February 23, 2017
©ESO 2017

TFAW: wavelet-based signal reconstruction to reduce photometric noise in time-domain surveys

D. del Ser[1,2], O. Fors[3,4], J. Núñez[1,2], N. M. Law[3], H. T. Corbett[3], J. K. Ratzloff[3], and W. S. Howard[3]

[1] Dept. de Física Quàntica i Astrofísica, Institut de Ciències del Cosmos (ICCUB), Universitat de Barcelona, Martí Franquès 1, E08028 Barcelona, Spain
e-mail: danieldelser@icc.ub.edu
[2] Observatori Fabra, Reial Acadèmia de Ciències i Arts de Barcelona, Rambla dels Estudis, 115, E-08002 Barcelona, Spain
[3] University of North Carolina at Chapel Hill, Department of Physics and Astronomy, Chapel Hill, NC 27599-3255, USA
e-mail: ofors@unc.edu
[4] Institut de Ciències del Cosmos (ICCUB), Universitat de Barcelona (IEEC-UB), Martí i Franquès 1, 08028 Barcelona, Spain

Received XXXX, XXXX; accepted XXXX, XXXX

arXiv:1702.06547v1 [astro-ph.IM] 21 Feb 2017

ABSTRACT

Context. There have been many efforts to correct systematic effects in astronomical light curves to improve the detection and characterization of planetary transits and astrophysical variability in general. Algorithms like the Trend Filtering Algorithm (TFA) use simultaneously-observed stars to measure and remove the systematic effects, and binning is used to reduce high-frequency random noise.
Aims. We present TFAW, a modified version of TFA which reduces the high-and-low-frequency noise in variable-star light curves without modifying their intrinsic characteristics.
Methods. We modified TFA's iterative signal reconstruction by adding a Stationary Wavelet Transform filter which characterizes the noise- and trend-free signal and the underlying noise contribution at each iteration. The algorithm performs an adaptive noise estimation through the wavelet transform which reduces correlated and uncorrelated noise while preserving signals typical of astrophysical changes. We carried out a series of tests over simulated sinusoidal and transit-like signals to assess the effectiveness of the method, and applied TFAW to real light curves from the Evryscope and TFRM. We also studied TFAW's application to simulated multiperiodic signals.
Results. The TFAW improvement in RMS of simulated and real light curves ranges from 0.025 to 0.05 magnitudes compared to TFA. The signal-detection frequency power spectra remain almost unchanged for high SNR light curves, confirming that TFAW does not introduce new correlated noise sources. The signal detection efficiency of the power-spectrum peaks improves by a factor ~1.5 for low SNR light curves, allowing the recovery of transiting planets smaller than previous algorithms. TFAW is also able to improve the characterization of multiperiodic signals. We present two newly-discovered variable stars from Evryscope and TFRM.
Conclusions. TFAW improves on the performance of trend-filtering algorithms by allowing adaptive binning to reduce the effects of correlated and uncorrelated noise. TFAW is a generic algorithm which is applicable to any kind of ground-based or space-based time-domain survey.

Key words. Methods: data analysis – Planets and satellites: detection – Planets and satellites: fundamental parameters – (Stars): planetary systems – Stars: variables: general – Surveys

1. Introduction

The photometric precision and accuracy achieved by an astronomical survey is a key factor in transit signal detection. The photometric precision that can be attained depends on several factors such as the atmosphere conditions, the instrument, the number of non-distorted stellar PSFs that can be imaged on the CCD, the reduction pipeline and the photometric errors of the measurements. Detectors with wide field of view (FoV) often suffer from additional issues such as undersampled PSFs, atmospheric extinction, source blending and optical distortion at the edges of the detector. These and other effects increase the noise of the light curves and also introduce systematic variations that decrease the detection probability of any periodic signal in the data.

Many of the systematic variations in a given light curve are shared by light curves of other stars in the same data set. In order to remove those systematics, one can identify the objects in the field that suffer from the same kind of variations as the target (correlated noise) and then build and apply a filter based on the light curves of these comparison stars. TFA and SysRem (Tamuz et al. 2005) are often applied to remove systematic variations in time-domain surveys, in particular wide FoV and/or multi-telescope transiting exoplanetary surveys, such as SuperWASP (Pollacco et al. 2006), MEarth (Irwin et al. 2009), HAT-South (Bakos et al. 2009), TFRM-PSES (Fors et al. 2013) or NGTS (Wheatley et al. 2013). All-sky surveys such as the Evryscope (Law et al. 2015, 2016) require robust systematics removal over extremely wide fields and petabyte-scale datasets.

The Trend Filtering Algorithm (hereafter TFA) (Kovács et al. 2005) implements correlated noise removal using multiple stars in the field. The first part of the algorithm consists of removing trends from trend- and noise-dominated time series in order to increase the probability of detecting weak signals (called frequency analysis in the original article). Secondly, if a significant periodic signal is present in the target light curve,

TFA reconstructs the shape of that signal using an iterative process (called signal reconstruction). One key aspect of the signal reconstruction step is that it should minimize the chances of suppressing the signal or modifying its intrinsic astrophysical characteristics. Several efforts have extended TFA to improve the signal recovery, such as using a meticulous selection of the reference stars (for example, Kim et al. 2009 through hierarchical methods or Principal Component Analysis, Petigura & Marcy 2012), or taking into account stellar variability or multiperiodic signals (Kovács & Bakos 2008). TFA is further described in Sect 2.1.

The TFA modification we present here (hereafter TFAW) introduces a wavelet filter in order to 1) estimate the shape of the trend- and noise-free phase folded signal and 2) iteratively denoise the trend-free light curve during the signal reconstruction process. TFAW combines TFA detrending and systematics removal capabilities with the wavelet transform's signal decoupling and denoising potential. The filter is built using the Stationary Wavelet Transform algorithm (hereafter SWT) or *à trous* algorithm (Holschneider et al. 1989).

The SWT and TFAW are described in Sect 2.2 and Sect 2.3 respectively. In Sect 3.1, we apply TFA and TFAW to sinusoidal and transit-like simulated light curves affected by combinations of Gaussian and correlated noise. The performance of the algorithms is compared in Sect 2.3, using the intrinsic light curve shape, the SNR of the light curve, and the standard Box Least Square (BLS) (Kovács et al. 2002) and Lomb-Scargle (LS) (Scargle, J. D. 1982)) periodograms. In addition, the application of the algorithm to multiperiodic superimposed signals is studied in Sect. 3.2. We apply TFAW to light curves from two independent real data sets from The Evryscope and the Telescope Fabra-ROA at Montsec (TFRM) in Sect 4.1 and Sect 4.2, respectively, to confirm that TFAW offers improved performance compared to TFA. Two of the light curves detrended with TFAW, one from Evryscope and one from TFRM, were found to be newly-discovered variable stars. In Sect. 4.3 TFAW vs. TFA comparative performance is quantitatively shown.

2. The TFAW algorithm

2.1. TFA basics and formulation

The key point behind TFA (Kovács et al. 2005) is the assumption that many stars within a photometric data set suffer from the same or similar systematic effects. Taking a representative set of reference stars, one can build a filter function that the removal of correlated systematics from a target light curve. Given a target N-point light curve and a set of M zero-averaged reference stars $\{X_j(i); i = 1, 2, ..., N; j = 1, 2, ..., M\}$, the filter for that target is defined as:

$$F(i) = \sum_{j=1}^{M} c_j X_j(i), \tag{1}$$

The set of coefficients $\{c_j\}$ is determined by minimizing the following expression:

$$D = \sum_{i=1}^{N} [Y(i) - A(i) - F(i)]^2, \tag{2}$$

Where $\{Y(i)\}$ represents the target light curve and $\{A(i)\}$ is either constant in the case of the frequency analysis step of the algorithm or, the best representation of the trend- and noise-free signal to be found in the iterative signal reconstruction step. Once the filter has been computed, the corrected light curve is defined by:

$$\hat{Y}(i) = Y(i) - \sum_{j=1}^{M} c_j X_j(i), \tag{3}$$

Although TFA is able to remove trends and systematics from photometric time series, this algorithm does not completely decouple stochastic and correlated noise from the underlying signals.

2.2. The Discrete Wavelet Transform and the Stationary Wavelet Transform

Unlike the Fourier transform, the wavelet transform decomposes a given time series into its *wavelets*, i.e., highly localized impulses obtained from scaling and shifting the *mother wavelet* function. These scaling and shifting operations allow us to calculate the wavelet coefficients, which represent the correlation between the wavelet and a localized section of the signal. The wavelet coefficients are calculated for each wavelet segment, giving a time-series function measuring the wavelets' correlation to the signal. In comparison to the sine wave used in the Fourier transform, which is smooth and of infinite length, the wavelet is irregular in shape and compactly supported. These properties make wavelets an ideal tool for analyzing signals of a non-stationary nature. Their irregular shape allows us to analyze signals with discontinuities or sharp changes, while their compactly supported nature allows temporal localization of the signal's features.

In the Discrete Wavelet Transform (DWT) the signal is decomposed into dyadic blocks (i.e. shifting and scaling is based on a power 2). The DWT of a given signal is calculated by applying a series of filters to the signal. In the first level of decomposition the signal passes through a low pass filter resulting in a convolution of the original signal and the filter. Simultaneously, the signal is also decomposed using a high-pass filter. The outputs give us the *detail coefficients* (related to the high-pass filter) and the *approximation coefficients* (related to the low-pass filter). The filter outputs are then sub-sampled by 2. In an iterative process, the original signal is then successively decomposed into components of lower scale, while the high frequency components are retained but not further decomposed. The decomposition is represented as a binary tree with the nodes representing a sub-space with a different time-frequency localization. The tree is known as a filter bank while the wavelet multi-scale decomposition and reconstruction is known as multi-resolution analysis (MRA) (Mallat 1989). The maximum number of decomposition levels that can be performed is dependent on the input size of the data: a signal of length 2^N can be decomposed into N discrete levels.

The DWT is not a time-invariant transform and is therefore very sensitive to the alignment of the signal in time (the DWT of a translated version of a signal might not be the translated version of the DWT of the signal). The Stationary Wavelet Transform (SWT) is a wavelet transform algorithm designed to overcome the lack of translation-invariance of the DWT. As with the DWT, high and low pass filters are applied to the signal at each level. However, in order to achieve translation-invariance, the downsamplers and upsamplers are removed and the filter coefficients are upsampled by a factor of $2^{(j-1)}$ in the jth level of

the algorithm. By padding the filters at each level with zeroes, the two new sequences at each level have the same length as the original time series.

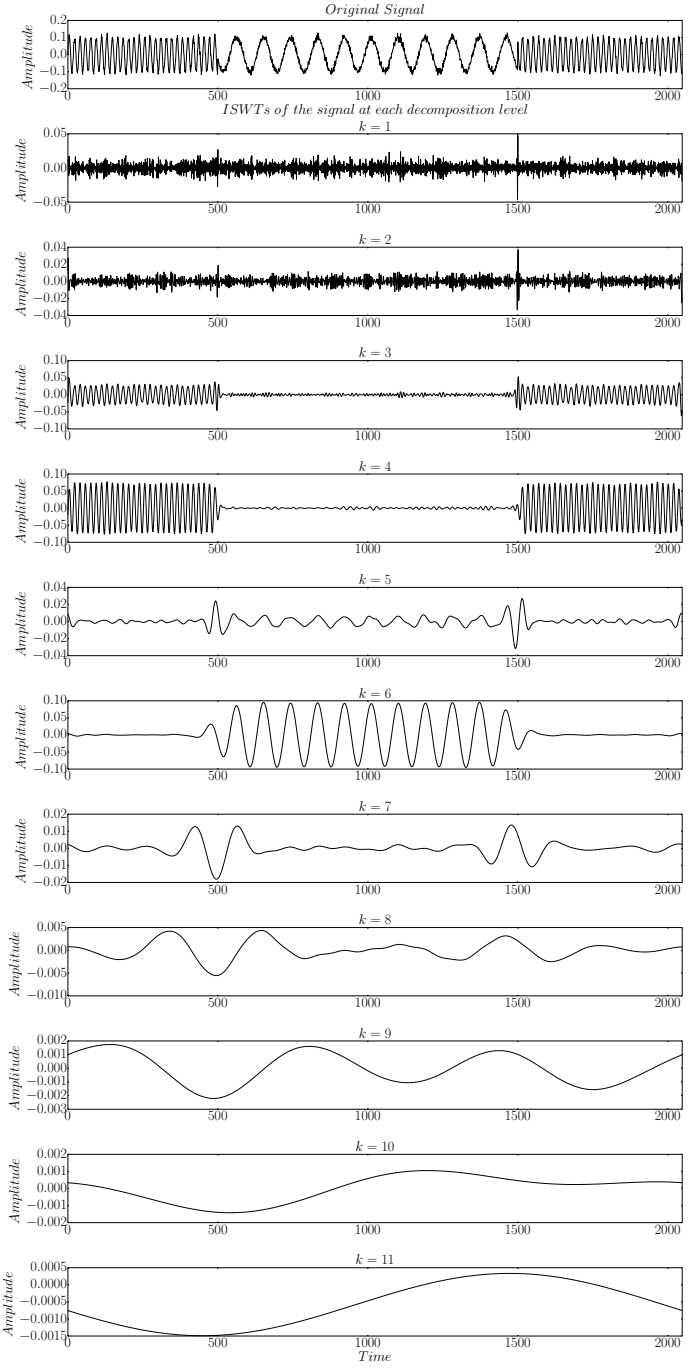

Fig. 1: SWT decomposition of a test signal. The uppermost plot shows the test signal as described in Section 2.2, consisting of two sinusoidal signals and Gaussian random noise. The plots following plots represent the ISWT transform of the signal at each SWT decomposition level (k = 1,...,11).

An example of a MRA using the SWT is shown in Figure 1. Our test signal is a combination of two sinusoidal signals, one of high frequency and another of low frequency. They both have the same amplitude and are affected by Gaussian random noise. As can be seen in Figure 1, SWT is able to decouple each of these signal contributions at different decomposition levels. This is shown by computing the inverse SWT (hereafter ISWT) at each level. High-frequency noise has been separated from the sinusoidal signals, appearing as an extra contribution to the higher decomposition levels. The noise can be fairly represented by the combination of the first two decomposition levels. The high frequency sinusoidal signal can be recovered by summing the third and fourth decomposition levels while the low frequency one would be recovered through the combination of the remaining levels. Crucially, the wavelet decomposition allows the signal characteristics to change through the time series, while retrieving both time and frequency information from the original signal. Other techniques such as the discrete Fourier Transform convert data from time into frequency domain but in doing so, time information is lost.

2.3. TFAW: application of the SWT

In the original version of TFA (Kovács et al. 2005), once a significant periodic signal has been found in the target time series during the frequency analysis step, the phase-folded light curve is used to iteratively estimate $\{A(i)\}$ (the noise-free signal). They employ the simple bin average method, using a fixed number of bins (100 for ∼3000 data points) to ensure statistical stability and to obtain a reasonable noise averaging. They point out, however, that more accurate methods can be used to approximate $\{A(i)\}$. For example, in the case of planetary transits, one could use a Mandel & Agol (2002) model fit to get a more precise estimation of the noise- and trend-free signal.

In TFAW we follow a similar approach to the original TFA. First, an initial filter is computed using $\{A(i)\} = \langle Y \rangle$. Then, we use BLS to search for any periodic signal within the filtered data. If any significant period is found, the light curve is phase folded to that period. Instead of using a bin average, $\{A(i)\}$ is estimated using the SWT of the phase folded signal. We decompose the phase folded light curve up to a SWT decomposition level given by the following equation:

$$max\ scale = \lfloor \frac{\log(\frac{n}{l-1})}{\log 2} \rfloor, \tag{4}$$

where n is the signal length and l is the wavelet filter length.

At each decomposition level, we set all the *detail coefficients* and *approximation coefficients* to zero except the ones corresponding to that level. Then, the ISWT is computed for each level separately (as seen in Figure 1). In order to estimate the shape of the noise- and trend-free signal we set a threshold decomposition level or *signal level* (see details in Section 2.4). $\{A(i)\}$ is then computed as the sum of the ISWTs of those levels from *signal level* to the last decomposition level. In this way we ensure that our signal estimate is separated from the high frequency noise while preserving the high-frequency shape of the signal (unlike normal binning): the high frequency noise components are better characterized by the upper decomposition levels as they have higher frequency resolution.

This new $\{A(i)\}$ can then be used to compute a new set of $\{c_j\}$ coefficients by means of equation 2. The new filter obtained from this set of coefficients gives us the new corrected light curve at each step of iteration through equation 3. We set an additional filter at each iteration given by the SWT of the phase folded light curve. In this case, instead of using those levels below *signal level* to reconstruct the noiseless signal, we set a *noise level* so

that the noise is characterized by the sum of the ISWTs of those levels above it. Thus equation 3 at each iteration step becomes:

$$\hat{Y}'(i) = \hat{Y}(i) - ISWT(\hat{Y(i)}, noise\ level), \quad (5)$$

The iteration of the algorithm stops when the relative difference between the standard deviations of the residuals in the successive iterations falls under a certain limit. As with the original TFA algorithm, we set the limit at 10^{-3}.

2.4. Signal and noise level choice criteria

The selection of the *signal level* and *noise level* parameters must be carefully performed. As described above, high-frequency noise appears as an extra contribution to the higher decomposition levels of the SWT. However, high frequency signals hidden within the data (i.e. second order sinusoidal modulations, etc...) could be present in some of the levels in which the noise also appears. One way of solving this issue would be to increase the number of data points to a higher power of two. The greater the number of levels into which we can decompose our signal, the easier it is to separate the noise contribution from the high frequency signals. Nonetheless, even if part of the signal is mixed with the noise at some level, using TFA signal reconstruction capabilities, one could be able to recover the signal without any distortion given that the correct period has been found except in those cases in which the frequency of the signal is exactly the same frequency as the noise.

One way to diminish the signal contribution lost at each iteration step and avoid any signal distortion is to select a *noise level* value that uses just the higher SWT decomposition levels (usually the highest one), and accept the noise contribution from the lower decomposition levels. We recommend setting a *noise level* equal to 1 (highest SWT decomposition level) for time series shorter than 2048 points (i.e. 10 decomposition levels) and increase it with care for each extra power of two of the time series length.

Regarding the *signal level*, given that it should provide the best estimation of the noise and trend-less signal, we recommend using a value around half of the maximum SWT decomposition level of the signal (given by equation 4). We set this value to, at least, the fourth to sixth lower decomposition levels (depending on the data length) to ensure the removal of most noise contributions but also to diminish both the chance of modifying the shape or removing part of the signal.

2.5. Mother wavelet selection criteria

There are several mother wavelets with different analytic properties that can be used for signal decomposition. For our application of the SWT-modified version of TFA we use the non-orthogonal, symmetric base of the biorthogonal (bior) wavelet family, first constructed by Cohen et al. 1992. More specifically, we used the pre-computed values of the bior 3.9 wavelet included in the PyWavelets module[1]. We selected this wavelet family for TFAW as it allows the construction of symmetrical wavelet functions and because the shape of the reconstruction scaling function in the case of the bior 3.9 wavelet is very similar to the characteristic shape of a planetary transit (searches for other types of astrophysical variability may benefit from other wavelet shapes).

[1] `https://pywavelets.readthedocs.io`

3. TFAW performance

3.1. Simulated data

In Kovács et al. 2005 several tests are presented demonstrating the signal detection and reconstruction capabilities of TFA. In this section we explore how the TFAW inclusion of the SWT filter can improve the SNR of the light curves, the impact this filter has on the BLS power spectra, and we compare the results with the ones obtained using the original TFA. For all the simulated light curves hereafter and the real ones in Section 4.1 and Section 4.2 we have used 2048 datapoints and set the *noise* and *signal levels* to the lower decomposition level and the five higher ones respectively. As stated in Section 2.3, this way we diminish the chances of losing part of the signal contribution when doing the noise estimation and produce an optimized noise- and trend-reduced signal estimation for these datasets.

To illustrate the noise and trend filtering efficiency of the TFAW method, we generate a sinusoidal signal affected by a combination of different levels of simulated Gaussian, σ_w, and correlated, σ_r noises. We also introduce linear and exponential trends (i.e. to simulate changes in airmass, changes in the CCD position of the object, etc) as well as gaps and jumps in the data. The period of the simulated signal is 0.63 days and 0.03 mag amplitude. We use a template of 250 simulated reference stars suffering from the same trends and systematics as the target star, each of them affected by a random distribution of σ_w and σ_r combinations (see Table 1 for details).

Table 1: Noise parameters for the simulated light curves

Signal type	SNR	σ_w (mag)	σ_r (mag)
Sinusoidal	High	0.01	0.005
Sinusoidal	Low	0.1	0.05
Transit	High	0.01	0.005
Transit	Low	0.04	0.005

Figure 2 shows the noise filtering capabilities of the TFA and the TFAW for a simulated target star with a sinusoidal modulation. While the noise dispersion has been clearly diminished, there has been no modification to either the amplitude or the phase of the signal, and the sampling timescale of the signal remains unchanged (unlike in simple binning). The BLS power spectrum as well as the height and amplitude of the peaks for the TFAW filtered signal have remained practically unchanged compared to the TFA ones.

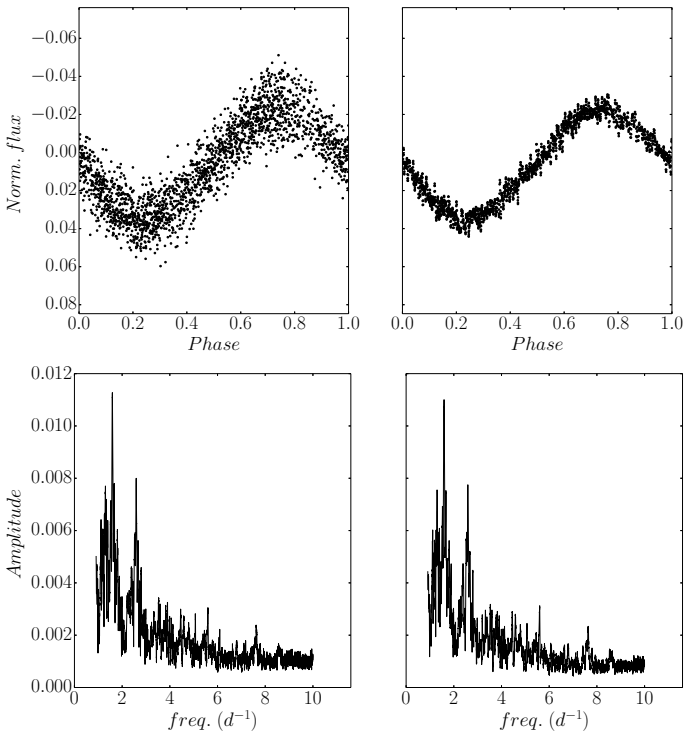

Fig. 2: Noise filtering comparison of a simulated sinusoidal signal. The same number of template stars and BLS parameters were used for TFA and TFAW. **Top left:** TFA-filtered phase folded signal. **Top right:** The same phase folded signal but TFAW-filtered. **Bottom left:** BLS power spectrum of the TFA-filtered light curve. **Bottom right:** BLS power spectrum of the TFAW-filtered light curve

In Figure 3, the same sinusoidal signal has been simulated but with lower SNR. As before, the noise dispersion has also significantly diminished while the period and amplitude of the signal have remained unchanged. In this case, however, the BLS power spectrum has improved and is much closer to the high SNR one (compare this power spectrum with the one in Figure 2; the noise floor has been greatly reduced). This improvement in the BLS power spectrum produces an improved signal detection efficiency (SDE) (Kovács et al. 2002) for the peak corresponding to the true period of the simulated signal.

Table 2: Planet parameters used for TFAW simulations

Planet	R_P (R_J)	M_P (M_J)	M_* ($M_\odot$)	R_* ($R_\odot$)	P (days)
1	1.98	1.40	1.36	1.23	0.8468
2	1.23	1.10	1.36	1.23	0.4842

Figure 4 simulates a planetary transit. We used VARTOOLS (Hartman 2016) and the parameters of planet 1 in Table 2 to simulate a Mandel & Agol (2002) planetary transit model, adding noise. The high-frequency noise is filtered by TFAW to give a better defined transit shape without modifying its shape or transit parameters. Like the first simulated sinusoidal signal, the TFAW BLS power spectrum for this high SNR planetary transit remains almost unchanged with respect to the TFA version, because the BLS power spectrum is not primarily limited by high-frequency random noise.

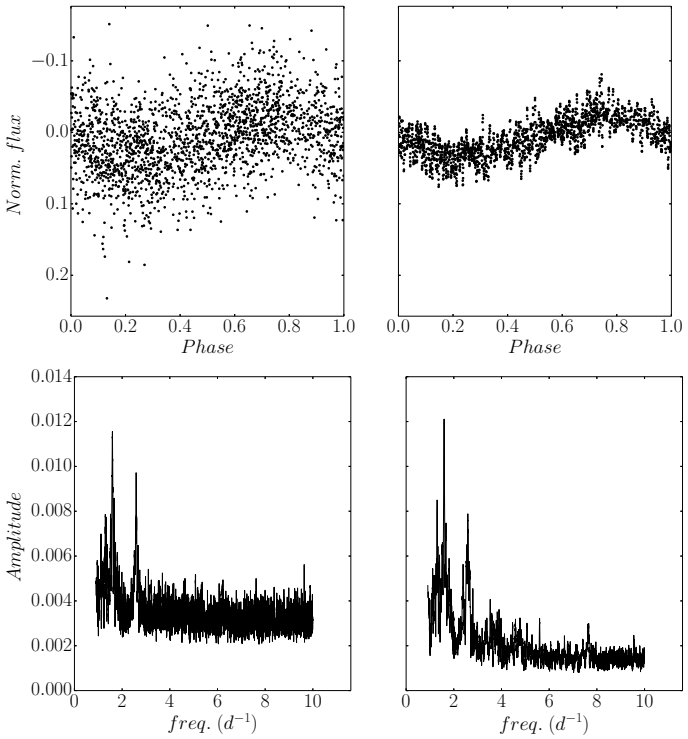

Fig. 3: Noise filtering comparison of a simulated sinusoidal signal with lower SNR. Same notation and TFAW parameters as Figure 2.

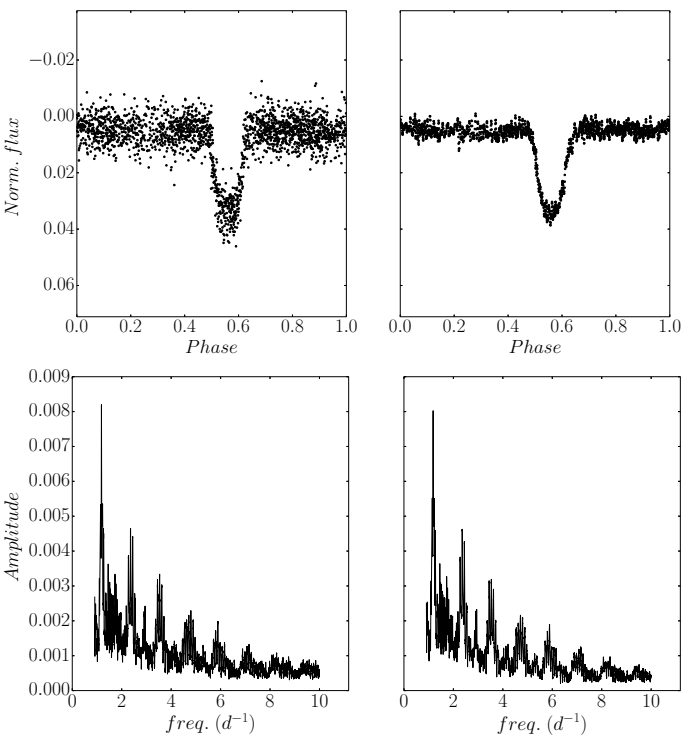

Fig. 4: Noise filtering comparison of a simulated box-shaped transit (planet 1 in Table 2). Same notation and TFAW parameters as Figure2.

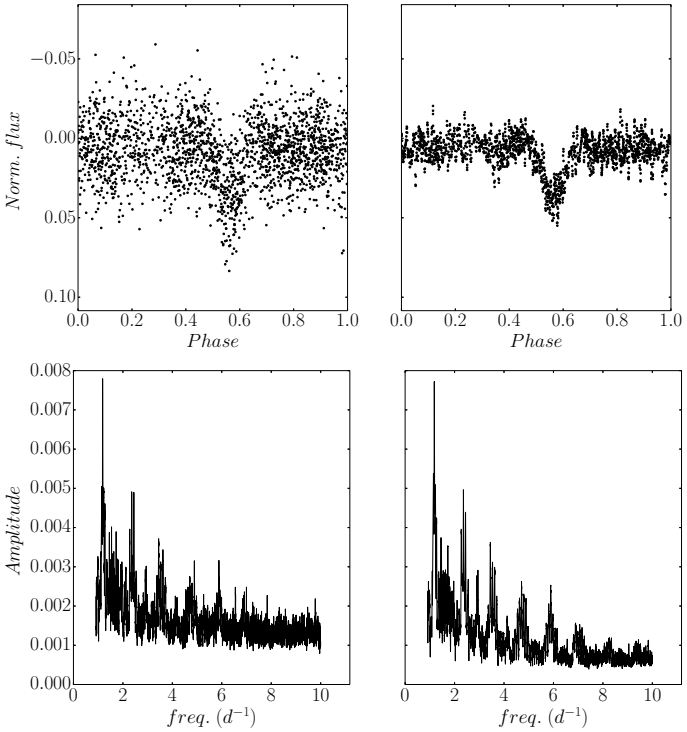

Fig. 5: Noise filtering comparison of the same simulated box-shaped transit as in Figure 4 with lower SNR. Same notation and TFAW parameters as Figure 2.

Figure 5 shows the same transit but with a much larger noise component. As in the case of the simulated sinusoidal with low SNR (see Figure 3), TFAW improves the characterization of the signal's shape while diminishing the noise, recovers the correct period and transit parameters, and improves the detectability of the transit signal in the BLS periodogram.

3.2. Application to multiperiodic signals

Kovács & Bakos (2008) presents a variation of TFA to extend its application to multiperiodic signals using their Fourier representation (for the cases in which such representation is adequate). However, they state that if the signal has additional components such as transients or planetary transits, a more complicated model should be used to approximate each of those extra signals present in the light curve. TFAW can be used to separate the different signal contributions directly from the signal after TFA's frequency analysis step (provided that the periods of each of the signals have been previously and correctly determined using BLS or another method). As a first example, we simulate the same sinusoidal signal as in Figure 2 and Figure 3 modulated with a 0.1438-day sinusoid with an amplitude of 0.006 mag. As can be seen in Figure 6, if we are able to find the correct frequency of the secondary signal (notice the peak around 6.9 d^{-1} in the corresponding BLS peridogram), we can fully recover it by applying TFAW directly to the raw data without modifying the amplitude, shape and period of any of the underlying signals.

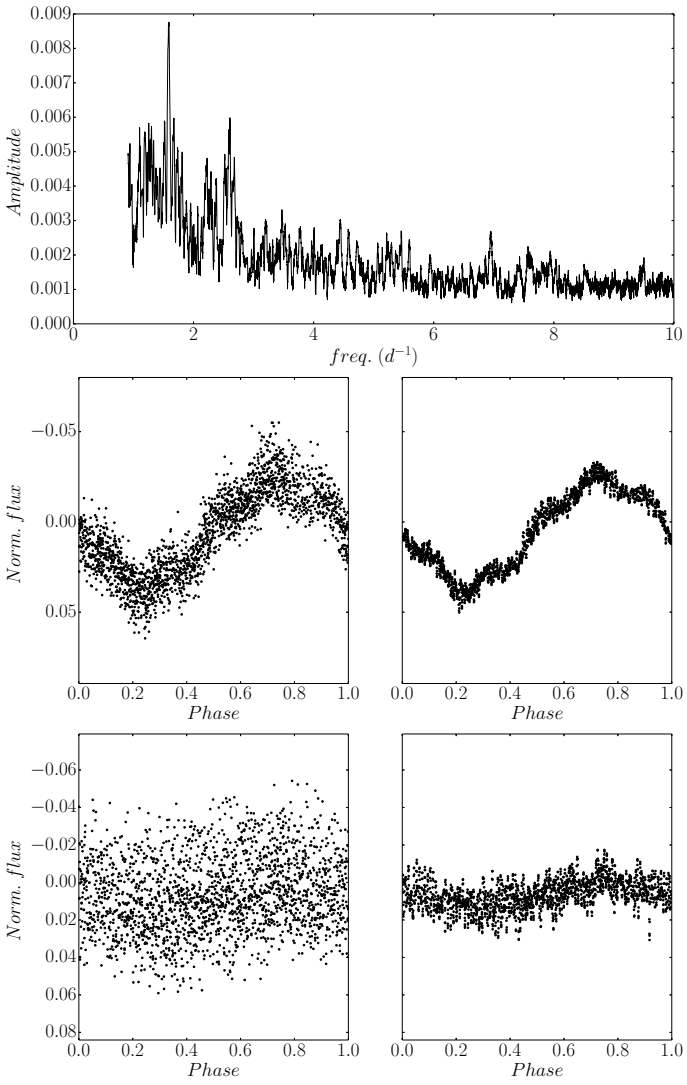

Fig. 6: Example of the signal recovery for a multi-periodic sinusoidal signal. **Top:** BLS power spectra of the signal after TFA frequency analysis step (notice the small peak around 6.9 d^{-1} corresponding to the secondary signal). **Middle left:** TFA phase-folded low frequency signal. **Middle right:**Same TFAW-filtered phased folded low frequency signal. **Bottom left:** TFA phase-folded secondary signal. **Bottom right:** TFAW phase-folded secondary signal.

The second example in Figure 7 shows the results of applying TFAW to a light curve affected by two planetary transits simulated with VARTOOLS and using the parameters of planets 1 and 2 in Table 2. Again, if we are able to find the period of the secondary transit after the frequency analysis step, we can separate the secondary transit from the primary simply by phase folding the raw light curve and applying TFAW. As in the other examples, we are also able to improve the SNR of both the primary and secondary signals.

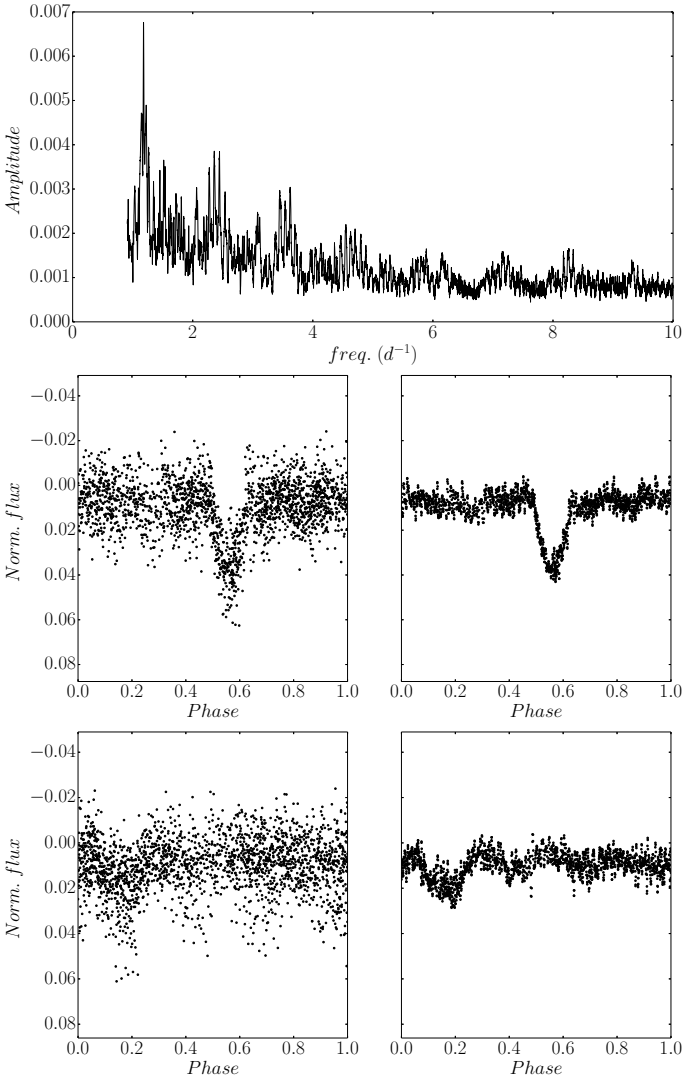

Fig. 7: Example of the signal recovery in a multi-transit light curve. **Top:** BLS power spectra of the signal after TFA frequency analysis step. Check the peak around 2 d^{-1} corresponding to the secondary transit. **Middle left:** TFA phase-folded planet 1 signal. **Middle right:** Same TFAW-filtered phased folded planet 1 signal. **Bottom left:** TFA phase-folded planet 2 signal. **Bottom right:** TFAW phase-folded planet 2 signal.

4. Application to Real Survey Light Curves

In this section we test the TFAW algorithm on real data from two ground-based surveys.

4.1. The Evryscope

The Evryscope (Law et al. 2014, 2015, 2016) is a telescope which covers the entire accessible sky above an airmass of 2 and is designed to be sensitive to exoplanetary transits and other short timescale events not discernible from existing large-sky-area astronomical surveys. The Evryscope consists of a single hemisphere containing twenty-three 61mm-aperture telescopes. The hemisphere tracks the sky on a standard German Equatorial mount, imaging a 691 MPix instantaneous 8,000 sq. deg. FoV, in two hour sections, ratcheting back after each chunk to cover a new sky area (with 75% overlap with the previous area). The system takes an exposure in g-band every 2 min, reaching a limiting magnitude of $g \sim 16$, and co-adds over hours each night to monitor fainter objects. The Evryscope is located at Cerro Tololo Inter-American Observatory (CTIO), covering declinations between $-90°$ and $+10°$. A Northern-Hemisphere Evryscope is to be deployed in 2017, monitoring the entire night sky at two-minute cadence.

4.1.1. Evryscope data analysis

The Evryscope data used for the TFAW performance assessment comprises 2048 data points observed from the 21^{st} of September 2016 to the 8^{th} of October 2016 with one of the Evryscope's telescopes. The initial data analysis used the standard Evryscope pipeline and database system (Evrypipe) (Fors et al. 2015a ,2015b). Briefly, the images are photometrically calibrated using standard techniques; the coordinates and instrumental magnitudes of all stars in the field are measured with SExtractor (Bertin & Arnouts 1996) using aperture photometry; and a custom astrometric solver is applied to map pixel coordinated to sky positions. The differential photometry calibration procedure for light curves first rejects frames with anomalous zero points, then picks an optimal photometric extraction radius for each star. In order to correct atmospheric extinction and other systematics, all light curves have had differential photometry applied using the BESTRED algorithm (Voss 2006) which, on a nightly basis, uses a set of the brightest, non-saturated and low RMS reference stars to compute the light curve corrections. Once the differential photometry has been applied, the magnitude residuals of the reference stars are fit with a second order polynomial to account for slowly-varying position-dependent effects. This fit is then applied to the rest of the light curves, before applying the TFAW algorithm.

4.1.2. Results

In Figures 8 and 9 we present two real examples comparing the results obtained with TFA and TFAW.

2MASS J13190996-8347115, a variable star discovered by the Evryscope, is a semi-detached contact binary of the W Ursae Majoris-type with a 0.658-day period. The TFAW-processed light curve is significantly less noisy than the TFA curve. The shape, depth and BLS power spectrum have not changed compared to TFA.

1RXS J031713.9-853231 is a strong magnetic field rotational white dwarf with a period of 725 sec and 0.2 mag peak-to-peak photometric variations, most likely to have spots (Kilic et al. 2015; Barstow et al. 1995; Ferrario et al. 1997). The target brightness is near the Evryscope single-image limiting magnitude, with expected photon-limited photometric errors around 10%. In this case, the signal is much clearer after TFAW has been applied and the BLS noise floor is reduced by a factor of ~ 3, making the harmonics of the signal much more detectable. For this star we find that the highest peak corresponds to the same period as the one found by Barstow et al. (1995) and Ferrario et al. (1997).

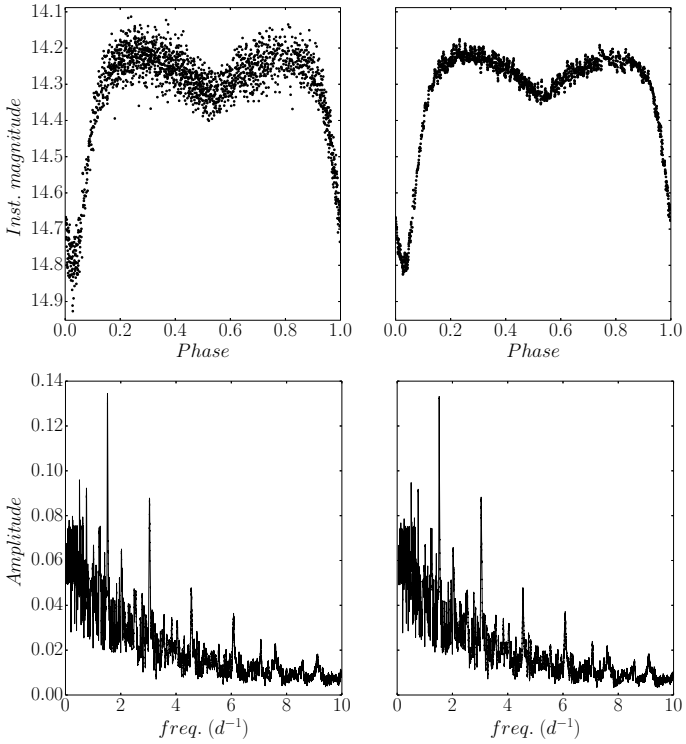

Fig. 8: Example of the TFAW filtering capabilities on the observed Evryscope light curve of 2MASS J13190996-8347115, a newly-discovered variable star. Same notation and TFAW parameters as Figure 2.

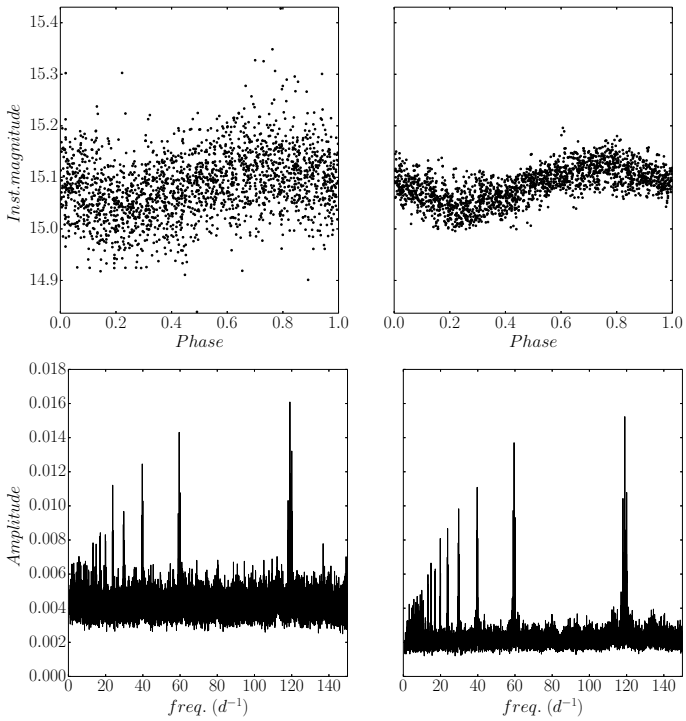

Fig. 9: Example of the TFAW filtering capabilities on the observed Evryscope light curve of white-dwarf 1RXS J031713.9-853231. Same notation and TFAW parameters as Figure 2.

4.2. The Telescope Fabra-ROA at Montsec

The Telescope Fabra-ROA at Montsec (TFRM) is a refurbished f/0.96 0.50m Baker-Nunn Camera (Henize 1957) for robotic CCD wide-FoV surveying purposes (Fors, et al. 2013). The project is a joint collaboration between the Reial Acadèmia de Ciències i Arts de Barcelona - Observatori Fabra and the Real Instituto y Observatorio de la Armada. The telescope is installed at the summit of the Montsec d'Ares (Spain) as part of the Observatori Astronòmic del Montsec.

The TFRM has been conducting a targeted M-dwarfs transiting exoplanetary survey (TFRM-PSES) since its deployment at the end of 2011. TFRM-PSES benefits from the wide FoV of 19.4 sq. deg. for a 16 MPix camera, and from the 0.1% -precision 20-second-cadence light curves for every object brighter than 16th magnitude (del Ser et al. 2015, Fors et al. 2013).

4.2.1. Data description

The data from the TFRM-PSES survey used for the TFAW performance assessment comprises 2048 data points from 30 nights observed during 2013, 2014 and 2015 for a field centered at (α, δ) = (10:14:44, +48:30:00). All light curves in the data set have been observed with a 475 nm cutoff frequency glass filter (Schott GG475), 17 sec exposure time and an altitude above 50 degrees. The light curves were generated with the APEX-2 reduction pipeline (Devyatkin et al. 2010). The pipeline includes aperture photometry, atmospheric extinction correction, differential photometry (using the BESTRED algorithm) and astrometric calibration.

4.2.2. Results

In Fig. 10 and Fig. 11 we present two examples obtained from the TFRM-PSES data. Fig. 10, 2MASS J10144313+5018191, is a newly-discovered variable star, probably a δ-Scuti star with a 0.3184-day period. As can be seen, after TFAW has been applied, the noise contribution has diminished significantly, the BLS power spectrum has remained almost unchanged, and there is a slight increase in the SDE of the peaks. The one in Fig. 11 is cataloged as NSVS 4921994 (Wozniak et al. 2004), a W Ursae Majoris-type variable star with a 0.371018-day period. As in the previous case, the SNR of the signal has improved and the correct period is recovered from the TFAW BLS power spectrum. It has to be noted that the qualitative difference in the overall BLS power spectrum of TFRM light curves compared to the ones coming from the Evryscope is due to the sampling of the data.

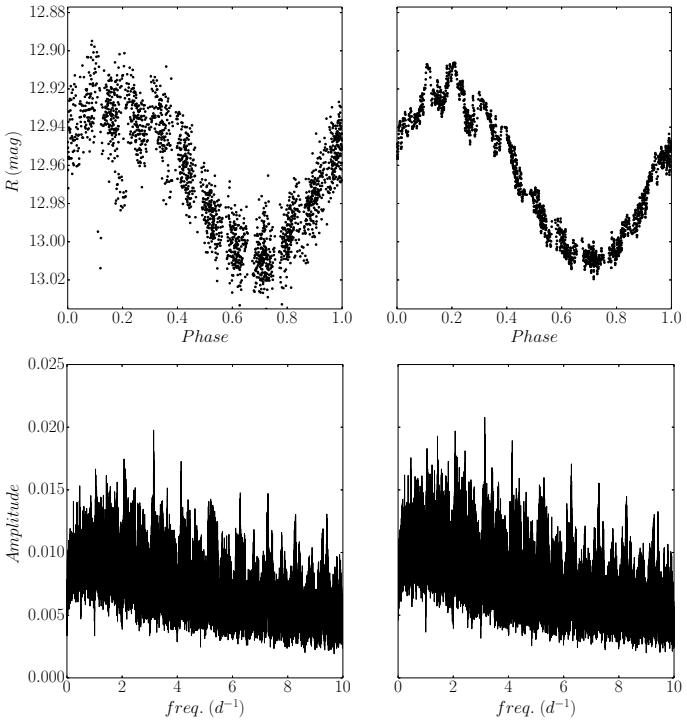

Fig. 10: Example of the TFAW filtering capabilities on the observed TFRM light curve of 2MASS J10144313+5018191, a newly-discovered variable star. Same notation and TFAW parameters as Figure 2.

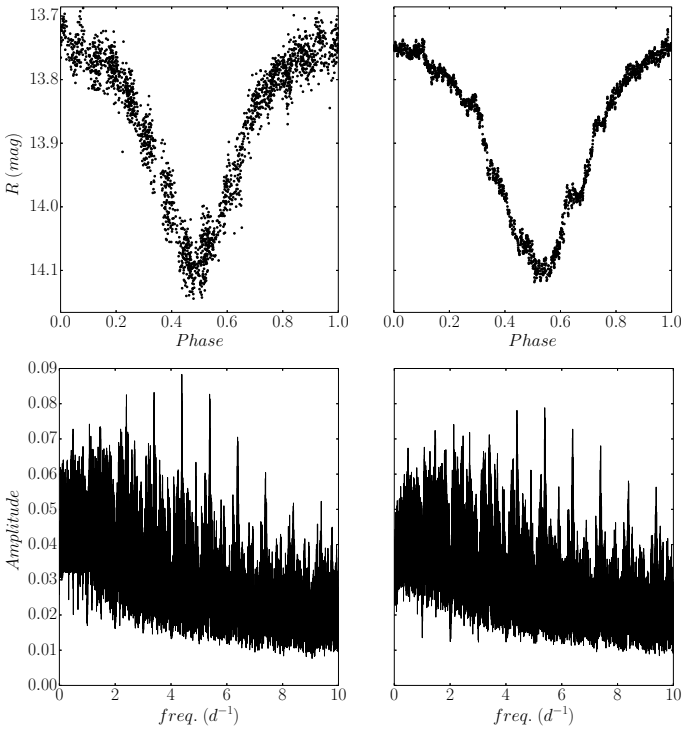

Fig. 11: Example of the TFAW filtering capabilities on the observed TFRM light curve of NSVS 4921994. Same notation and TFAW parameters as Figure 2.

4.3. TFAW quantitative performance

Tests made on both simulated and real light curves show that after TFAW has been applied, signals affected by systematics and noise can be recovered without their real shapes and periods being modified. Fig. 12 shows the decrease in the standard deviations of a sample of TFAW-filtered variable star light curves compared to the original TFA ones. Standard deviations have been computed for a set of Evryscope and TFRM variable stars (including the ones presented in Sects. 4.1.2 and 4.2.2). It can be seen that, with the increase in TFA standard deviation (conversely in raw magnitude), TFAW filtering capabilities lead to significant improvements in the standard deviation of the light curves. This improvement is usually around 0.025 magnitudes but sometimes, up to 0.05 or higher for low SNR light curves.

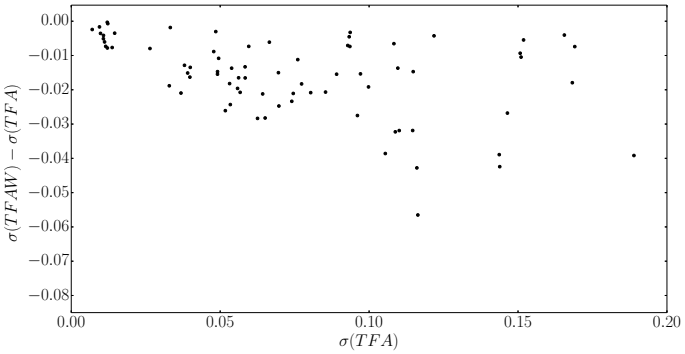

Fig. 12: Decrease of the standard deviations of the light curves of a set of variable stars due to the application of TFAW filtering, selected from light curves measured as part of the Evryscope and TFRM surveys.

The results shown in Sects. 4.1.2 and 4.2.2 on the BLS power spectra after TFAW-filtering show that TFAW does not introduce false periodicity or eliminate any of the periodogram peaks. For high-SNR TFAW-filtered light curves, where the BLS detections are limited by sampling and other issues, the BLS power spectra remains almost unchanged with respect to the TFA-filtered one. However, there is a clear improvement in the low SNR regime of about a factor 1.5 – 3, both in the overall power spectrum standard deviation and in the SDE of the peaks, produced by a reduction in the BLS noise floor.

In the case of multiperiodic light curves, TFAW is able to isolate the different underlying signals directly from the raw data provided that their corresponding periods have been correctly determined through BLS or any other method (like Lomb-Scargle). As for non-multiperiodic signals, each signal component can be recovered without modifying its shape or period while improving its SNR using TFAW noise-filtering capabilities.

Regarding the number of reference/template stars, tests run both with simulated and real light curves show that around 250 template stars gives the best results. TFAW can also be run with less stars (<10 stars). However, the noise filtering is less efficient and some trends and systematics could still be present in the filtered data. As with the original TFA, it is not necessary to compute the template matrix for each target star, only in the cases in which the latter accidentally coincides with one of the reference ones.

The algorithm has been fully implemented and parallelized in Python. The CPU time needed for a 2048 data points, single light curve TFAW analysis using a template of 250 reference

stars is typically around 60 seconds and about 100 iteration steps. A full run of the TFAW on 12,000 TFRM light curves with 2048 points per time series, 250 reference stars and 90000 BLS frequency steps took around 8 CPU hours using 24, 2GHz cores.

5. Conclusions

TFAW is a totally generic, Python-based, parallelized algorithm useful for any kind of survey which seeks to improve the performance of signal detection and reconstruction, provided that a set of comparison light curves sharing the same systematics and trends as the target time series is available. TFAW makes use of TFA's frequency analysis step to determine if a significant period is present in the data. If it exists, the use of the SWT allows a more precise estimation of the signal's shape. The algorithm then decouples a large component of the noise contribution from the raw signal, making use of a modified version of the original TFA iterative signal reconstruction approach, leading to an overall SNR improvement without alteration of the signal's time sampling or astrophysical characteristics.

TFAW shows an improvement of ~0.025 to 0.05 magnitudes (although it can be higher) in the standard deviations of the light curves with respect to the TFA ones, leading to a better characterization of the signal. Results obtained after studying the BLS power spectra of the TFAW-filtered light curves show that TFAW does not introduce any false periodicity, and that it can improve up to a factor 1.5 the overall BLS power spectra of non-multiperiodic signals and the SDE of the peaks.

It is important to note that TFAW needs an even number of data points to work that will depend on the number of levels in which the signal wants to be decomposed (ideally, the length of the time series should be a power of two). Also, as described in Section 2.3, better results are obtained if the number of SWT levels is above ten, ensuring that the noise and signal contributions are as separated as possible in the SWT decomposition of the signal. Compared to the original TFA, TFAW requires fewer reference stars to create the template used for the signal reconstruction and the noise filtering (Kovács et al. (2005) suggests the use of ~600 reference stars, while TFAW operates stably with 250 reference stars (in the data presented in this paper).

We have also shown that TFAW is able to isolate the different underlying signals within a light curve with multiple periodic signals, such as multi-transit signals, transients, modulations or other kinds of stellar variabilities. As for single-period light curves, the SNR of each each signal contribution improves due to the noise filtering capabilities of the TFAW.

In this paper we have applied TFAW to thousands of light curves from the Evryscope and TFRM. The TFAW algorithm also has the potential to improve the noise characteristics of space-based data sets, such as from Kepler or CoRoT; this study will be detailed in a following paper.

Acknowledgements. Daniel del Ser acknowledges financial support from RACAB and Universitat de Barcelona. The Evryscope component of this paper is supported by NSF/ATI AST-1407589, NSF/CAREER AST-1555175, and Research Corporation Scialog awards 23782 and 23822. The TFRM project is supported, in part, by the Departament d'Empresa i Coneixement de la Generalitat de Catalunya. We also acknowledge support by the Spanish Ministerio de Economía y Competitividad (MINECO/FEDER, UE) under grants AYA2013-47447-C3-1-P, AYA2016-76012-C3-1-P, MDM-2014-0369 of ICCUB (Unidad de Excelencia 'María de Maeztu'), and the Catalan DEC grant 2014 SGR 86. The authors would like to acknowledge Ignasi Ribas, Jaime Boloix, Albert Rosich, and Juan Carlos Morales for their contribution to the TFRM-PSES survey, as well as to the support team of the TFRM for the commissioning and maintenance of the telescope.

References

Barstow, M. A., Jordan, S., O'Donoghue, D., et al. 1995, MNRAS, 277, 971
Bertin, E. & Arnouts, S. 1996, SExtractor: Software for source extraction, A&AS 117, 393-404
Bakos, G., Afonso, C., Henning, T., et al. 2009, Transiting Planets, 253, 354
Cohen, A., Daubechies I. & Feauveau, J.-C. 1992, Biorthogonal bases of compactly supported wavelets, Communications on Pure and Applied Mathematics, 45, 5
del Ser, D., Fors, O., Núñez, J., et al. 2015, Living Together: Planets, Host Stars and Binaries, 496, 301
Devyatkin, A., Gorshanov, D., Kouprianov, V. & Verestchagina, I. 2010, Apex I and Apex II software packages for the reduction of astronomical CCD observations. Solar System Research, 44, 68-80
Djorgovski, S. G., Drake, A. J., Mahabal, A. A., et al. 2011, arXiv:1102.5004
Ferrario, L., Vennes, S., Wickramasinghe, D. T., Bailey, J. A. & Christian, D. J. 1997, MNRAS, 292, 205
Fors, O., Law, N. M., Ratzloff, J., et al. 2015, IAU General Assembly, 22, 2253010
Fors, O., Law, N. M., Ratzloff, J., et al. 2015, IAU General Assembly, 22, 2258237
Fors, O., Núñez, J., Muiños, J. L., Montojo, F. J., Baena-Gallé, R., Boloix, J., Morcillo, R., Merino, M., Downey, E. C. & Mazur, M. J., 2013, PASP, 125, 522
Hartman, J. D., Bakos, G., Stanek, K. Z., & Noyes, R. W. 2004, AJ, 128, 1761
Hartman, J. D. & Bakos, G.Á. 2016, VARTOOLS: A program for analyzing astronomical time-series data, Astronomy and Computing, 17, 1-72
Henize, K. G. 1957, S&T, 16, 108
Holger, V., Developing a ground-based search system for transits of extrasolar planets. Berlin: s.n., Phd thesis
Holschneider M., Kronland-Martinet R., Morlet J. & Tchamitchian P. 1989, A real-time algorithm for signal analysis with the help of the wavelet transform. In Wavelets, Time-Frequency Methods and Phase Space, 289–297
Irwin, J., Charbonneau, D., Nutzman, P., & Falco, E. 2009, Transiting Planets, 253, 37
Kaiser, N., Burgett, W., Chambers, K., et al. 2010, Proc. SPIE, 7733, 77330E
Keller, S. C., Schmidt, B. P., Bessell, M. S., et al. 2007, PASA, 24, 1
Kilic, M., Gianninas, A., Bell, K. J., et al. 2015, ApJ, 814, L31
Kim, D.-W., Protopapas, P., Alcock, C., Byun, Y.-I., & Bianco, F. B. 2009, MNRAS, 397, 558
Kovács, G., Zucker, S. & Mazeh, T. 2002, A&A, 391, 369
Kovács, G., Bakos, G. & Noyes, R. W. 2005, A trend filtering algorithm for wide-field variability surveys, MNRAS, 356, 557-567
Kovács, G., Bakos, G. 2008, Application of the Trend Filtering Algorithm in the search for multiperiodic signals, Communications in Asteroseismology, 157, 82-86
Law, N. M., Kulkarni, S. R., Dekany, R. G., et al. 2009, PASP, 121, 1395
Law, N. M., Fors O., Wulfken, P., Ratzloff, J. & Kavanaugh, D., 2014, The Evryscope: the first full-sky gigapixel-scale telescope, in Society of Photo-Optical Instrumentation Engineers (SPIE) Conference Series 9145, 0
Law, N. M., Fors O., Wulfken, P., Ratzloff, J., Kavanaugh, D., Sitar, D. J., Pruett, Z., Birchard, M. N., Barlow, B. N., Cannon, K., Cenko, S. B., Dunlap, B., Kraus, A. & Maccarone, T. J., 2015, Evryscope Science: Exploring the Potential of All-Sky Gigapixel-Scale Telescopes, PASP 127, 234-249
Law, N. M., Fors, O., Ratzloff, J., et al. 2016, Proc. SPIE, 9906, 99061M
Mallat S. G. 1989, A Theory for Multiresolution Signal Decomposition: The Wavelet Representation, IEEE Transactions on Pattern Analysis and Machine Intelligence, 11, 7
Mandel, K., & Agol, E. 2002, ApJ, 580, L171
Petigura, E. A., & Marcy, G. W. 2012, PASP, 124, 1073
Pollacco, D. L., Skillen, I., Collier Cameron, A., et al. 2006, PASP, 118, 1407
Scargle, J. D. 1982, Studies in Astronomical Time Series Analysis II: Statistical Aspects of Spectral Analysis of Unevenly Spaced Data, Astrophysical Journal, 263, 835-853
Tamuz, O., Mazeh, T., & Zucker, S. 2005, MNRAS, 356, 1466
Tonry, J. L. 2011, PASP, 123, 58
Woźniak, P. R., Vestrand, W. T., Akerlof, C. W., et al. 2004, AJ, 127, 2436
Wheatley, P. J., Pollacco, D. L., Queloz, D., et al. 2013, European Physical Journal Web of Conferences, 47, 13002